RSC Advances

ROYAL SOCIETY OF CHEMISTRY

www.rsc.org/advances

Journal Name

COMMUNICATION

Formation mechanism of spinel $LiTi_2O_4$ prepared by carbon thermal reduction reaction

Received 00th January 20xx,
Accepted 00th January 20xx

DOI: 10.1039/x0xx00000x

www.rsc.org/

Guijun Yang [a, b], Jianwen Yang [a, c*], Lingzhi Zhang [b*]

The formation mechanism of $LiTi_2O_4$, prepared by a carbon thermal reduction reaction using Li_2CO_3 and TiO_2 (anatase) as starting material and acetylene black as a reducing agent, was investigated by in-situ variable temperature X-Ray diffraction and thermal gravimetric analysis/differential scanning calorimetry system. It was found that the cooling rate significantly impacts on obtaining pure phase $LiTi_2O_4$ sample after forming $LiTi_2O_4$ product during the carbon thermal reduction reaction. $LiTi_2O_4$ has excellent cycling stability, remaining a specific capacity of 126.6/111.9 mAh g^{-1} with a capacity fade of 5.1%/3.1% at 0.5 C/1 C rate after 200 cycles.

In recent years, great efforts have been made to develop spinel-structured $Li_4Ti_5O_{12}$ as an alternative replacement for currently used graphite anode material in lithium-ion batteries (LIBs) due to its superior advantages such as high power capability, unique safety performance (1.55 V *vs*. Li/Li^+), and excellent cycling stability (zero-strain insertion material) [1,2]. But $Li_4Ti_5O_{12}$ has a poor electrical conductivity ($< 10^{-13}$ S cm^{-1}) which seriously limits its high-rate performances for practical applications [3]. Spinel $LiTi_2O_4$ has a similar crystal structure and lithium-ion migration path with $Li_4Ti_5O_{12}$ [4] and especially has a significantly higher electrical conductivity of 5.56×10^6 S cm^{-1} [5-7] compared with $Li_4Ti_5O_{12}$. These features make $LiTi_2O_4$ a more promising anode material as a replacement of $Li_4Ti_5O_{12}$ in lithium-ion batteries.

Various approaches have been explored to synthesize $LiTi_2O_4$, such as solid state reaction [8,9], sol-gel method [10,11], molten salts electrolysis [12,13], hydrothermal reaction [14]. Among of these methods, solid-state reaction usually uses titanium [5] or low-valence titanium oxides [15] as reductants or other reducing elements such as lithium or hydrogen [16]. However, most synthesis reported requires rigorous conditions, costly starting materials or dangerous hydrogen gas. Moreover, the synthesis of spinel $LiTi_2O_4$ with pure phase is difficult compared to $Li_4Ti_5O_{12}$, because of the existence of mixed valence state titanium ions (Ti^{3+} and Ti^{4+}) in $LiTi_2O_4$. In 2010, we reported an improved one-step carbon thermal reduction method to prepare $LiTi_2O_4$ using Li_2CO_3 and anatase as starting materials and acetylene black as a reducing agent [17]. Nonetheless, we have reproducible problem to prepare spinel $LiTi_2O_4$ with pure phase due to the unclear underlying mechanism during the solid state reaction.

In this work, we investigate the formation mechanism of $LiTi_2O_4$ in our one-step carbon thermal reduction reaction using *in-situ* variable temperature X-ray diffraction (VT-XRD) and thermal gravimetric analysis/differential scanning calorimetry system (TGA-DSC). The electrochemical performances of pure spinel $LiTi_2O_4$ are also reported.

In situ VT-XRD was carried out on a PANalytical X'Pert Powder diffractometer with Cu Kα radiation (λ=1.5405Å), equipped with an Anton Parr HTK 1200N high temperature attachment. The samples were heated in N_2 atmosphere from room temperature to 900℃ with a heating rate of 10℃/min, and then stabilized for 30 min at each integer point of temperature. SDTQ600 thermal gravimetric analysis/differential scanning calorimetry system was used to identify the phase transition temperature in N_2 atmosphere. The morphologies of the $LiTi_2O_4$ samples at different cooling rate were observed by SEM. ^{7}Li MAS NMR spectrum of $LiTi_2O_4$ was acquired on an AV 400 Bruker spectrometer under magic angle sinning at 5 kHz using 4mm zirconium rotors. CV was conducted in cells at 0.2 mV s^{-1} from 0.8 V to 2.5 V. EIS was measured by applying an alternating voltage of 5 mV over the frequency ranging from 10^2 to 10^5 Hz.

The *in situ* VT-XRD measurement was used to analyze the formation mechanism of $LiTi_2O_4$ during the carbon thermal reduction. The XRD patterns over heating from room temperature to 900℃ in a 2θ range of 10 °-70 ° are shown in Fig. 1a. The XRD patterns of the starting materials before heating are well consisted with the corresponding crystal structure in the database. The peaks

[a]College of Chemistry and Bioengineering, Guilin University of Technology, Guilin 541004, Guangxi, China
[b]Key Laboratory of Renewable Energy, Guangzhou Institute of Energy Conversion, Chinese Academy of Sciences, Guangzhou 510640, Guangdong, China
[c]Guangxi Key Laboratory of Electrochemical and Magneto-chemical Functional Materials, Guilin University of Technology, Guilin 541004, China
*Corresponding authors.
Tel.: +86 773 2538354; fax: +86 773 5896839.
E-mail address: yangjw@glite.edu.cn (Dr. J. W. Yang).
Tel.: +86 20 37246025; fax: +86 20 37246026.
E-mail address: lzzhang@ms.giec.ac.cn (Dr. L. Z. Zhang).
DOI: 10.1039/x0xx00000x

at 20.3 °, 35.8 ° and 43.4 ° corresponding to (0 2 0), (-1 3 1) and (2 0 2) plane of Li_2TiO_3 intermidiate started to appear at 600℃. At 700 ℃, the peaks at 35.5 ° and 40.3 ° corresponding to (3 1 1) and (4 0 0) plane of $LiTi_2O_4$ appeared, suggesting that $LiTi_2O_4$ product was generated since 700℃. The peak at 18° corresponding to (1 1 1) *plane of $LiTi_2O_4$ and Li_2TiO_3* was not distinguishable due to overlapping of these two phases. After heating to 800℃ and kept for 30 min, anatase disappeared completely. The intensity of rutile increased rapidly because of anatase turned into rutile from 700℃ to 800℃, and then decreased after 800℃ due to its continuous consumption by reacting with Li_2TiO_3 to generate $LiTi_2O_4$. In our experiments, rutile completely disappeared when the temperature was heated to 900℃ and kept for 12 h.

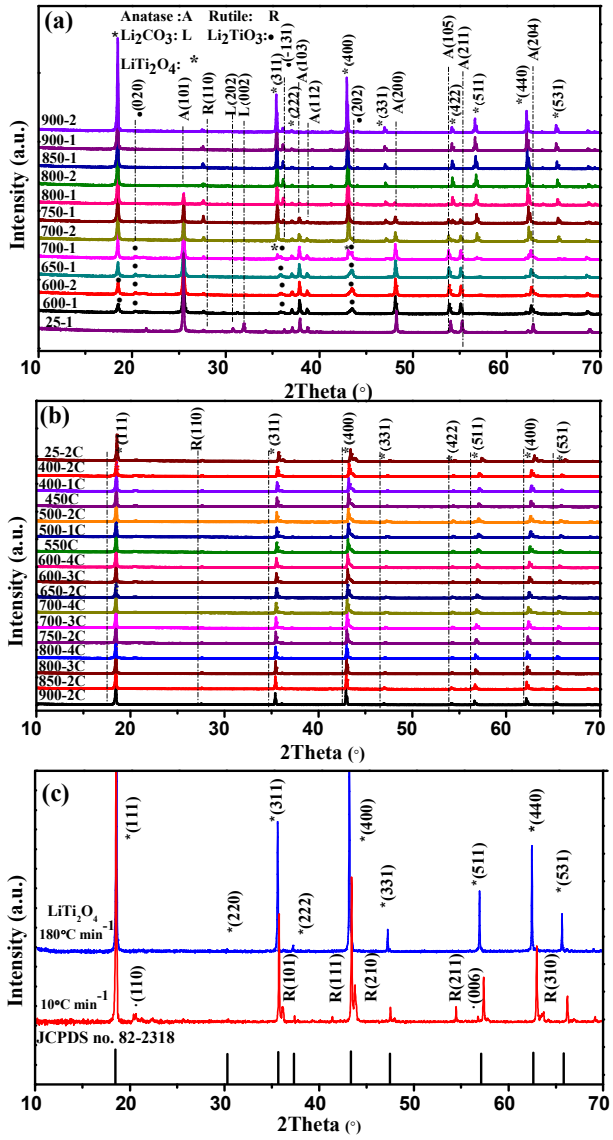

Figure 1. (a) The *in situ* VT-XRD patterns of $LiTi_2O_4$ during heating stage from room temperature to 900℃; (b) *in situ* VT-XRD patterns of $LiTi_2O_4$ during cooling stage from 900℃ to room temperature; (c) XRD pattern of $LiTi_2O_4$ during different cooling rate.

It worth to point out that the cooling rate has a significant impact on obtaining pure phase $LiTi_2O_4$ sample [18]. Fig. 1b shows the *in situ* VT-XRD patterns of $LiTi_2O_4$ product cooling from 900℃ to room temperature with a rate of 10℃ min^{-1}. As the temperature decreased after 850℃, the diffraction peaks of $LiTi_2O_4$ product shifted to larger angles, indicating that the impurity was generated in the product (Fig. 1b). A comparative experiment was conducted by cooling the $LiTi_2O_4$ product at different rate of 180℃ min^{-1} and 10℃ min^{-1}, respectively. At a fast cooling rate of 180℃ min^{-1}, the pure phase $LiTi_2O_4$ was obtained as a deep-blue powder with well-defined and sharp XRD diffraction peaks which is consistent well with the reference $LiTi_2O_4$ (JCPDS no. 82-2318, Fig. 1c). As comparison, impurity was observed after cooling at 10℃ min^{-1} as shown in Fig. 1c.

SEM observation shows that $LiTi_2O_4$ sample cooled at 180℃ min^{-1} has a size range of 400 to 500 nm with perfect cubic shape (Fig. S1a). As comparison, $LiTi_2O_4$ sample cooled at 10℃ min^{-1} has similar size, but consists of a lot of shapeless broken particles (Fig. S1b). The ^7Li MAS NMR spectrum of pure $LiTi_2O_4$ cooled at 180℃ min^{-1} displays only one chemical shift at -0.053ppm with three symmetric spinning sidebands at 42.957/-43.082, 85.727/-85.775, 128.510/-128.531 ppm (Fig. S1c), due to the average oxidation state of Ti^{3+} and Ti^{4+} ions in $LiTi_2O_4$ [18,19].

Based on the above results, the formation mechanism of $LiTi_2O_4$ was proposed as following, and schematically illustrated in Scheme 1:

$$Li_2CO_3 + TiO_2(anatase) \xrightarrow{600℃} Li_2TiO_3 + CO_2\uparrow \quad \text{(Equ.1)}$$

$$Li_2TiO_3 + 3TiO_2(anatase) + C \xrightarrow{700℃} 2LiTi_2O_4 + CO\uparrow \quad \text{(Equ.2)}$$

$$TiO_2(anatase) \xrightarrow{700℃} TiO_2(rutile) \quad \text{(Equ.3)}$$

$$Li_2TiO_3 + 3TiO_2(rutile) + C \xrightarrow{800℃} 2LiTi_2O_4 + CO\uparrow \quad \text{(Equ.4)}$$

$$LiTi_2O_4 \xrightarrow{\text{slowly decreasing}} Li_yTi_{3-y}O_4 (1 \le y \le 2) \quad \text{(Equ.5)}$$

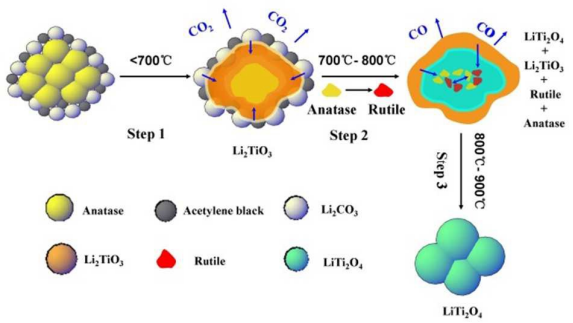

Scheme 1. Schematic formation mechanism of $LiTi_2O_4$.

TGA-DSC experiment was carried out from room temperature to 1000℃ to further confirm the formation mechanism of $LiTi_2O_4$ during the solid state reaction (Fig. 2). The TGA curve of the reaction mixture (Li_2CO_3, TiO_2 and acetylene black) for synthesizing $LiTi_2O_4$ showed a weight loss of 0.83% at a temperature range of room temperature to 500℃ due to the dehydration of the reactants which is correlated with the broad endothermic peak at the same temperature range in DSC curve. The second weight loss of 18.3% at 500℃-720℃ in TGA curve corresponds to the

exothermic peak at the same temperature range in DSC curve which composes of two relatively sharp exothermic peaks at 580℃-680℃ and 680℃-720℃, respectively. These two sharp exothermic peaks correspond to the Equ.1 reaction with a weight loss of 11.61 wt. % (fitting well with the theoretical value of 10.83 wt. %) and the Equ.2 reaction between Li_2TiO_3 and anatase with a weight loss of 6.69 wt. % (fitting well with the theoretical value of 7.01 wt. %), respectively.

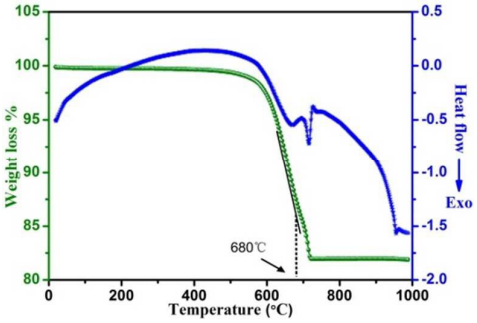

Figure 2. TGA-DSC curves of $LiTi_2O_4$ measured from room temperature to 1000℃.

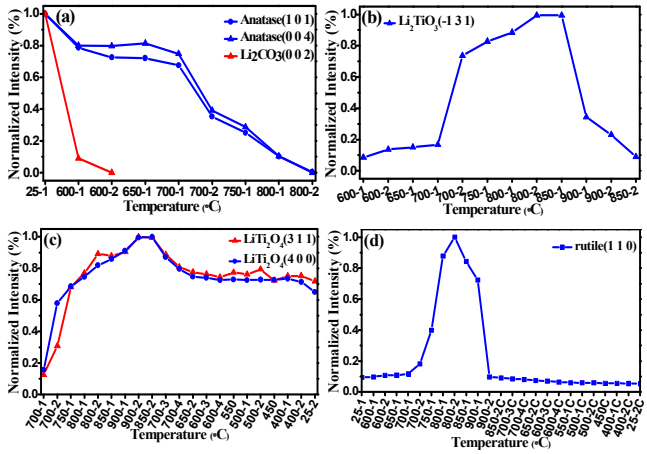

Figure 3. The normalized intensities of *in situ* VT-XRD peaks for (a) anatase, Li_2CO_3 (b) intermediate Li_2TiO_3 and (c) $LiTi_2O_4$ product and (d) rutile at the heating and cooling temperature.

To correlate with the previous XRD data, the intensities of *in situ* VT-XRD peaks for reactants, intermediate and product are normalized as shown in Fig. 3. The small sharp exothermic peak observed in Fig. 2 from 720℃ to 750℃ corresponds to the phase transformation of anatase to thermodynamically stable rutile in Equ.3. [20] Anatase disappeared completely at 800℃, evidenced by that the normalized intensity of anatase decreased to zero (800-2C in Fig. 3a). It is worth to note that Li_2TiO_3 continued to react with rutile to generate $LiTi_2O_4$ product after 800℃ (Equ.4) which correlates well with the intensity change of rutile, Li_2TiO_3 and $LiTi_2O_4$ product (Fig. 3b-3d). There is no obvious weight loss in TGA curve, mainly because of the very little amount of the rutile and the reaction is slow. Therefore, it is necessary to keep at 900℃ for 12 h in experiments to obtain the $LiTi_2O_4$ with pure phase.

CV and EIS measurements were used to characterize and compare the electrochemical kinetics of $LiTi_2O_4$ electrode at different cooling rates. Both samples display a pair of reversible oxidation and reduction peaks at 1.63/1.44 V and 1.86/1.33 V for $LiTi_2O_4$ cooled at 180/10℃ min^{-1}, respectively (Fig. S2a). But $LiTi_2O_4$ cooled at 180℃ min^{-1} shows relatively sharper peaks and smaller potential difference (ϕ_a-ϕ_b) of 0.19 V between anodic and cathodic peaks as compared with 0.53 V for $LiTi_2O_4$ cooled at 10℃ min^{-1}, suggesting a lower polarization of the electrode. The Nyquist plot for $LiTi_2O_4$ electrode at different cooling rate both consists of a semicircle and a linear part (Fig. S2b); the fitted parameters including the electrolyte resistance (R_s), the charge-transfer resistance (R_{ct}), the double layer capacitance and passivation film capacitance (CPE), the exchange current density (i^0=RT/nFR_{ct}) are collected in Table S1. [21] These data, together with the above CV results, imply that $LiTi_2O_4$ sample cooled at 180℃ min^{-1} has an improved electrical conductivity and better electrochemical kinetics as compared with $LiTi_2O_4$ sample cooled at 10℃ min^{-1}.

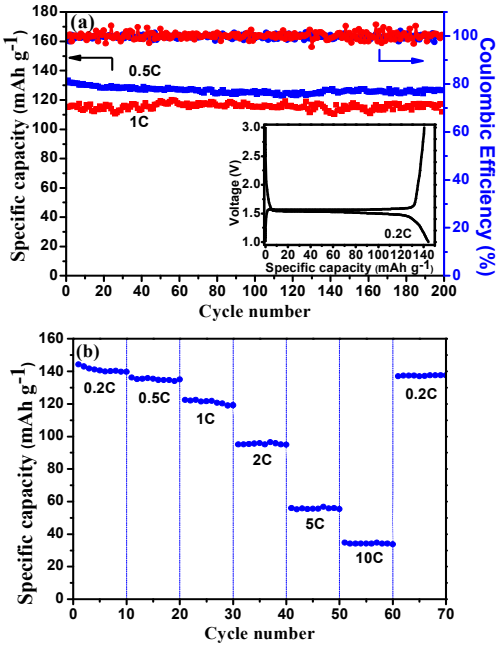

Figure 4. (a) The cycling performance of $LiTi_2O_4$ during 180℃ min^{-1} cooling at 0.5 C/1 C rate and (b) rate capability

The voltage-capacity curve for the initial charge/discharge cycle at 0.2 C is shown as the inset in Fig. 6a. The potential profile of $LiTi_2O_4$ electrode exhibited a typical long and flat potential plateau at around 1.55 V (vs. Li/Li^+), corresponding to the lithium insertion/extraction reaction between $LiTi_2O_4$ and $Li_2Ti_2O_4$ phase. At 0.2 C rate, the electrode showed a reversible discharge capacity of 144.5 mAh g^{-1} with a coulombic efficiency of 98% between 1.0 and 3.0 V. The long-term cycling performances of $LiTi_2O_4$ electrode at 0.5 C and 1 C rate are displayed in Fig. 4a. The $LiTi_2O_4$ electrode showed an initial charge capacity of 133.4/115.1 mAh g^{-1} at 0.5 C/1 C rate, respectively. Over 200 cycles, $LiTi_2O_4$ electrode remarkably retained a stable cycling capacity of 126.6/111.9 mAh g^{-1} with corresponding capacity retention of 94.9%/96.9% at 0.5 C/1 C rate, respectively. These data are better, in terms of capacity and cycling stability, than those of spinel $LiTi_2O_4$ samples recently reported in literature, [22,23] even including that doped with metal ions (Fe and V).

[24,25] Fig. 4b shows the rate capability of the $LiTi_2O_4$ electrode. The current density was increased gradually from 0.2 C to 10 C and then returned back to 0.2 C. When the rate increased from 0.2 C to 5 C, the $LiTi_2O_4$ electrode maintained an average reversible capacity of 54.3 mAh g^{-1}. When the current density was returned back to 0.2 C, a stable reversible capacity of 137.5 mAh g^{-1} was obtained, which is about 95.2% of the initial charge capacity at 0.2 C, indicating that the integrity of $LiTi_2O_4$ electrode was maintained even after high rate charge and discharge tests.

Conclusions

The formation mechanism of $LiTi_2O_4$ in the one-step solid-state reaction using Li_2CO_3 and TiO_2 (anatase) as starting material and acetylene black as reductant is studied by *in situ* VT-XRD measurements and TGA-DSC analysis. The formation of spinel $LiTi_2O_4$ consists of three steps. Firstly, Li_2CO_3 reacts with TiO_2 (anatase) to form intermediate Li_2TiO_3. Secondly, Li_2TiO_3 reacts with TiO_2 (anatase) in the presence of acetylene black to form $LiTi_2O_4$ at 700℃. In the same time, anatase starts to transform into rutile at 700℃. Thirdly, Li_2TiO_3 continues to react with TiO_2 (anatase and rutile) and acetylene black to generate $LiTi_2O_4$ product. Interestingly, the cooling rate significantly impacts on obtaining pure phase $LiTi_2O_4$ sample. Pure $LiTi_2O_4$ sample can be reproducibly prepared as a deep-blue powder at a fast cooling rate of 180℃ min^{-1}. Comparative CV and EIS study shows that $LiTi_2O_4$ cooled at 180℃ min^{-1} has improved electrical conductivity and favorable electrochemical kinetics as compared with the sample cooled at 10 ℃ min^{-1}. The electrochemical investigation shows that $LiTi_2O_4$ exhibits excellent cycling stability with a capacity retention of 96.9% at 1 C after 200 cycles. We believe that this work will construct a solid foundation for optimizing the synthesis and further developing $LiTi_2O_4$ as anode material for lithium-ion batteries.

Supporting information

Details of the synthesis, characterization, and electrochemical measurements.

Acknowledgments

This work was supported by National Natural Science Foundation of China (51164006/21573239), CAS Key Laboratory of Renewable Energy (Y407K41001), Science & Technology Program of Guangxi Province (1298025-9), Special Support Program of Guangdong Province for High-Level Talents (2014TX01N014), Collaboration Project of CAS-Guangdong Province (2013B09 1300017) and Guangzhou Municipal Project for Science & Technology (201423/2014Y2-00219).

Notes and references

1 T. Ohzuku, A. Ueda, N. Yamamoto, J. Electrochem. Soc., 1995, **142**, 1431-1435.

2 G. Q. Zhang, B. Y. Xia, C. Xiao, L. Yu, X. Wang, Y. Xie and X. W. Lou, Angew. Chem. Int. Ed., 2013, **52**, 8643-8647.

3 Q. Y. Zhang, H.S. Lu, H.X. Zhong, X. D. Yan, C. Y. Ouyang, L. Z. Zhang, J. Mater. Chem A, 2015, **3**, 13706-13716.

4 T. F. Yi, Y. Xie, Y. R. Zhu, J. Power Sources, 2012, **198**, 318-321.

5 K. M. Colbow, J. R. Dahn, R. R. Haering, J. Power Sources, 1989, **26**, 397-402.

6 A. Kuhn, C. Baehtz, F. Garcia-Alvarado, J. Power Sources, 2007, **174**, 421-427.

7 H. X. Geng, A. F. Dong, G. C. Che, W. W. Huang, S. L. Jia, Z. X. Zhao, Physica C, 2005, **432**, 53-58.

8 M. Manickam, M. Takata, J. Power Sources, 2003, **114**, 298-302.

9 J. A. Mergos, C. T. Dervos, Mater. Charact., 2009, **60**, 848-857.

10 L. Persi, F. Croce, B. Scrosati, Electrochem. Commun., 2002, **4**, 92-95.

11 M. Łapiński, B. Kościelska, W. Sadowski, J. Phys. Chem. Solids, 2013, **74**, 575-578.

12 N. Kumada, M. H. K. Rubel, A. Miura, T. Takei, J. Ceram. Soc., 2014, **122**, 307-309.

13 J. Akimoto, Y. Gotoh, K. Kawaguchi, Y. Oosawa, J. Solid State Chem., 1992, **96**,446-450.

14 D. Fattakhova, V. Petrykin, J. Brus, T. Kostlánová, J. Dědeček, P. Krtil, Solid State Ionics, 2005, **176**, 1877-1885.

15 A. Kuhn, M. Martín, F. García-Alvarado, J. Solid State Chem., 2010, **183**, 20-26.

16 T. Kanno, J. Awaka, F. Kariya, S. Ebisu, S. Nagata, Physica B: Condensed Matter, 2006, **381**, 30-33.

17 J. W. Yang, J. Zhao, Y. Z. Chen, Y. Li, Ionics, 2010, **16**, 425-429.

18 J. P. Kartha, D. P. Tunstall, John T. S. Irvine, J. Solid State Chem., 2000, **152**, 397-402

19 C. P. Grey, N. Dupre, Chem. Rev. 2004, **104**, 4493-4512.

20 K. J. D. Mackenzie, P. J. Melling, Trans. J. Brit. Ceram. Soc., 1974, **73**, 179-183.

21 L. Yue, S. Q. Wang，X. Y. Zhao, L. Z. Zhang, J. Mater. Chem., 2012, **22**, 1094-1099

22 C. Q. Feng, L. Li, Z. P. Guo, J. Alloy. Compd., 2009, **478**, 767-770.

23 M. J. Pan, Y. X. Chen, H. B. Liu, Ionics, 2015, **21**, 2417-2422

24 S. Chakrabarti, A. K. Thakur, K. Biswas, Solid State Ionics, 2014, **262**, 49-55

25 J. Liu, C. Q. Du, Y. Q. Lin, Z. Y. Tang, X. H. Zhang, J. Alloy Compd. 2015, **622**, 250-253

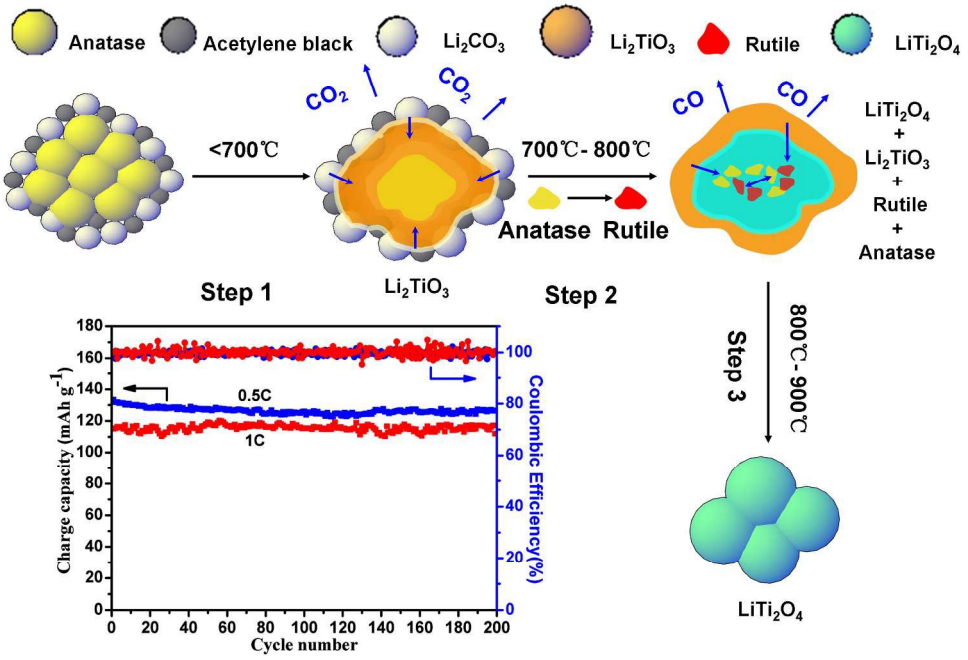

Graphical Abstract